INTERNATIONAL JOURNAL OF INTELLIGENT CONTROL AND SYSTEMS
VOL. 13, NO. 1, MARCH 2008, 15-24

Slip Angle Estimation for Lunar and Planetary Rovers

Giulio REINA and Kazuya YOSHIDA

***Abstract*— Vehicle slip is a critical issue for mobile robots driving across loose soil. It is responsible for gradual deviation of the vehicle from the intended course, resulting in large drift and poor performance of localization and control systems, even leading, in extreme cases, to the danger of vehicle entrapment with consequent mission failure. This paper presents a novel method for lateral slip estimation based on visually observing the trace produced by the wheels of the robot, during traverse of soft, deformable terrain, as that expected for lunar and planetary rovers. The proposed algorithm uses a robust Hough transform enhanced by fuzzy reasoning to estimate the angle of inclination of the wheel trace with respect to the vehicle reference frame. Any deviation of the wheel trace from the planned path of the robot suggests occurrence of sideslip that can be detected, and more interestingly, measured. This allows the vehicle to estimate its actual heading angle, usually referred to as the slip angle. The details of the various steps of the visual algorithm are presented and the results of experimental tests performed in the field with an all-terrain rover are described, proving the method to be effective and robust.**

***Index Terms*— Rough-terrain mobile robotics, planetary rovers, slip angle estimation, visual tracking of wheel trace.**

I. INTRODUCTION

The mobility of a robot driving across soft soils, such as sand, loose dirt, or snow, is greatly affected by slipping and skidding. As demonstrated by the Mars exploration of the NASA/JPL rovers Spirit and Opportunity [1], wheel slippage is a dominant disturbance on sandy slopes. This precludes the use of conventional dead-reckoning techniques for navigation, since they are based on the assumption that wheel revolutions can be translated into correspondent linear displacements. Thus, if one wheel slips, then the associated encoder will register revolutions even though these revolutions do not correspond to a linear displacement of the wheel. Conversely, if one wheel skids, fewer encoder pulses will be counted. Slippage not only affects the odometric accuracy, but increases the overall energy consumption and reduces the robot's traction and climbing performance, possibly resulting in large drift. The availability of a sensory system able to estimate slip would be greatly beneficial to a mobile robot, so that its odometry-based pose estimation could be compensated and corrective control actions may be executed, such as planning an alternate route away from a low-traction terrain region, or implementing a traction control algorithm [2]. Additionally, accurate position estimation is required for efficient and robust map building.

Most of the research in the field of mobile robotics has been focusing on the study of slip along the longitudinal direction of motion. Longitudinal slip can be estimated through the use of encoders by comparing the speed of driven wheels to that of undriven wheels [3]; however this does not apply for all-wheel drive vehicles or those without redundant encoders. Reina *et al* [4], proposed measures for longitudinal slip detection, based on comparing different onboard sensor modalities within a fuzzy logic inference engine. Ojeda *et al* [5], presented a motor current-based slip estimator, while in [6], a Kalman filter-based approach combining encoders, IMU, and GPS was discussed for detecting immobilization conditions of a mobile robot. However, in the presence of side forces, the robot moves at an angle (i.e. the slip angle) with respect to its longitudinal axis, resulting in lateral slip as well [7]. Thus, it is very important to address the issue of measuring the combined lateral and longitudinal slip. A large body of research work exists in the automotive community related to traction control, anti-lock braking systems (ABS), and electronic stability program (ESP); however, these works generally apply to asphalt roads and at significantly higher speeds than those typical for autonomous robots [8], [9]. In this area, Kalman filters have been widely applied to inertial and absolute measurements, such as GPS, to enhance dead reckoning and estimate lateral slip [10], [11]. However, GPS is not available for planetary applications, nearby trees and buildings can cause signal loss and multipath errors, and changing satellites can cause position and velocity jumps [12]. Additionally, GPS provides low frequency updates (e.g. typically near 1 Hz) making GPS alone too slow for accurate slip detection.

This paper investigates the feasibility of a novel approach for slip angle estimation developed for mobile robots traveling on loose terrain, such as that planetary rovers are expected to encounter. The general approach is based on using a rear video camera to observe the pose of the trace, (defined later), that is produced by the wheels, and detect whether the robot follows the desired path or deviates from it because of slippage. Figure 1 shows a direct example that will help to clarify this approach, believed to be proposed here for the first time. For the extensive testing of the system during its development, we employed the rover El Dorado, built at the Space Robotics Laboratory of the Tohoku University and also shown in Fig. 1. The rear webcam, mounted to a frame attached to the vehicle's body, is visible in the same figure. El Dorado is an independently controlled 4-wheel-drive/4-wheel-steer mobile robot, also featuring a typical rocker-type suspension system. Its operational speed ranges from 2 to 30

Manuscript received October 15, 2007; revised February 16, 2008. This work was supported by the JSPS Fellowship program. A part of this paper was accepted for presentation at the IEEE International Conference on Robotics and Automation, Pasadena, Ca, USA, May 2008.

G. Reina is with the Department of Innovation Engineering, University of Salento, 73100 Lecce, Italy. Email: giulio.reina@unile.it

K. Yoshida is with the Department of Aerospace Engineering, Tohoku University, Aoba 6-6-01, 980-8579 Sendai, Japan. Email: yoshida@astro.mech.tohoku.ac.jp

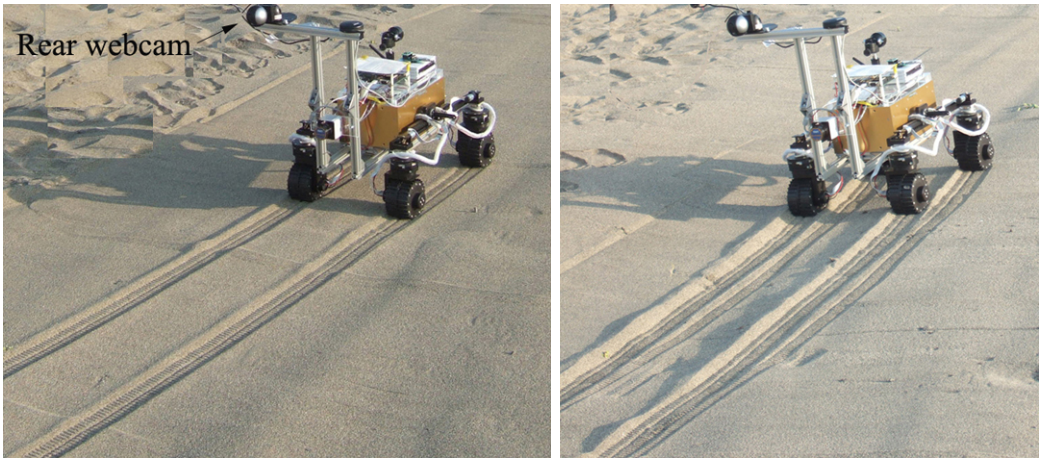

(a) (b)

Fig. 1. Sideslip estimation on sandy terrain by visual observation of the wheel traces with a rear webcam: (a) wheel traces parallel to the direction of motion, no lateral slip, (b) wheel traces inclined with respect to the intended direction of motion, significant lateral slip

cm/s. The robot is equipped with wheel and steer encoders, a fluxgate compass to measure the absolute vehicle heading, a rear-mounted camera and other sensors such as laser range finder and GPS that are not employed for this application. Figure 1(a) shows El Dorado as driving up a sandy slope following a straight path without any significant sideslip. This is shown by two distinct traces parallel to the direction of motion and produced by the wheel pair of either side of the robot. In Fig. 1(b), El Dorado negotiates a sandy slope with a contemporary transverse inclination, as also shown by the slight roll angle of the robot. The consequent external side force acting on the rover results in a substantial lateral drift. The traces, left by the wheels of the same side of the robot, are no longer superimposed and, most importantly, their angle of inclination, with respect to a reference frame attached to the vehicle, differs from the case of absence of slip. The proposed approach aims at estimating the slip angle of the robot by measuring the pose of one of the wheel traces, i.e. the rear left wheel, in conjunction with the knowledge of the rate-of-turn provided by the onboard compass.

Somewhat related research has been devoted to the study of lane departure warning systems and automated highways. A wide variety of techniques has been employed aiming at developing efficient and robust lane detectors based on visually observing white road markings on dark and relatively uniform background [13], [14]. In previous research [15], a method for lane tracking was presented. In this paper a similar approach is extended and optimized for the special case of tracking wheel traces on sandy terrain. Since our approach is based on Hough transform supported by Fuzzy logic to provide robust and accurate tracking of the wheel Trace, we call it FTrace.

The paper is organized as follows. Theoretical and experimental description of the FTrace module is provided in Section II. In Section III, the system is proved to be effective and robust in field tests performed with the rover El Dorado. Section IV concludes this paper.

II. The FTrace system

Tracking the trace of a wheel can turn into a very complex problem especially when shadows, occlusions, and terrain unevenness come into play. A robust and efficient trace detection system must be able to filter out all disturbances and extract the marking of interest from a non-uniform background in order to produce an accurate and reliable estimate of the trace pose relative to the vehicle. In Fig. 2, a sample image set demonstrates the variety of terrain and environmental conditions that can be encountered. Figure 2(a) shows a scene where trace detection can be considered relatively easy thanks to the clearly defined imprint and uniform terrain texture. In Fig. 2(b), extraction of wheel trace is more difficult due to the presence of transverse line-like discontinuities of the terrain. Figure 2(c) shows a non-uniform terrain texture, whereas in Fig. 2(d) and Fig. 2(e) a more complex wheel trace is shown due to presence of heavy shadowing. Finally, Fig. 2(f) refers to a condition where two imprints are present in the same scene.

The FTrace module performs wheel trace tracking based on a robust Hough transform enhanced by fuzzy logic. The relevant geometrical properties extracted from the scene are combined based on in-depth physical understanding of the problem. In this section, a theoretical analysis of the method is presented, providing also experimental evidence of its effectiveness.

A. Theoretical Analysis

1) Model Building: The presence of a rear camera mounted on the vehicle body is assumed, with a field of view on the ground plane corresponding to a 60 cm long $\times$ 80 cm wide area, behind the left rear wheel. It is also considered that the location of the camera relative to the wheel is known and fixed during travel. Under the assumption that the

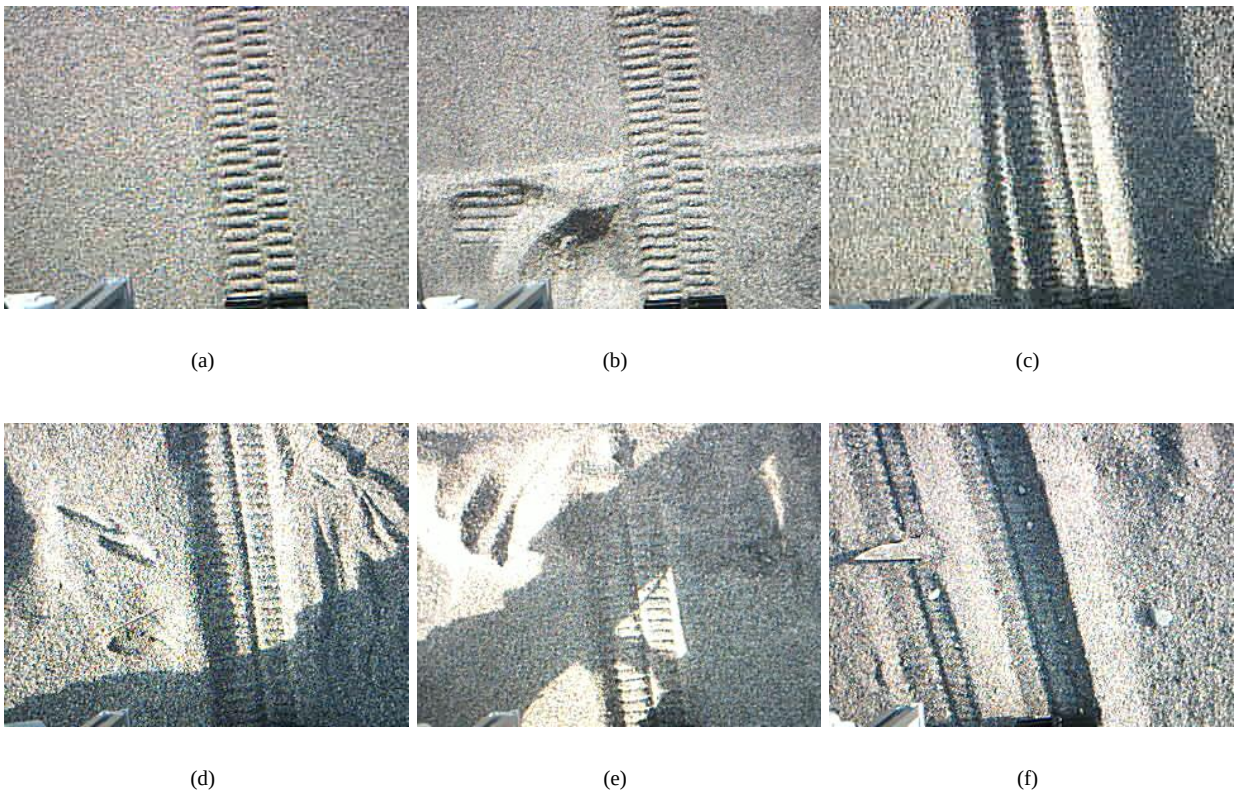

Fig. 2. Sample images of terrain and wheel trace conditions: (a) uniform sandy terrain, (b) disturbances due to transversal line-like discontinuities, (c) non-uniform terrain texture, (d) and (e) non-uniform terrain texture with noise due to shadowing, (f) different imprints present in the scene

portion of the trace in the image and the amount of sideslip is relatively small between two consecutive image frames acquired at fixed time interval during rover motion, the trace curvature can be neglected and it is possible to refer to a trace model composed of a single line, corresponding to its centerline. In the image plane of the camera, the model pose is defined by the two polar parameters ρ and φ, as shown in Fig. 3. In the real world, we can refer to a simple schematic of the vehicle, known as the bicycle model [16], and shown in Fig. 4. The bicycle model neglects weight transfer from inner to outer tires and assumes the same tires and slip angles on the inner and outer wheels. The trace pose is defined by the distance d_t with respect to the center of mass of the vehicle G, and the angle θ_t between the velocity vector of the rear wheel, V_r, and the wheel longitudinal axis. This angle is also usually referred to as the slip angle of the rear wheel α_r. Moreover, since the trace originates from the wheel-ground interface, an additional constraint can be formulated in the real world: the trace must always pass through the center of the wheel, i.e. point B in Fig. 4. With reference to the same figure, we can formally define the slip angle β of the vehicle as the angle between the velocity vector V of its center of mass G and the longitudinal axis X_v. Under the assumption of small angles, the following linearized relations hold between the slip angles and the velocity components

$$\beta = \frac{V_y}{V_x} \tag{1}$$

$$\alpha_r - \delta_r = \frac{V_y - r \cdot b}{V_x} = \beta - \frac{b}{R_t} \tag{2}$$

where V_x, V_y are the longitudinal and lateral component of the velocity vector V, δ_r is the rear steer angle, r is the rate-of-turn expressed in rad/s, R_t, defined as $R_t = V_x/r$, represents the distance of the instantaneous center of rotation from the longitudinal axis of the vehicle, and b is the distance between the rear axis and the center of mass G.

From (2), it is possible to estimate the slip angle β, given α_r from the FTrace module, δ_r and V_x from the steer and wheel encoders, and r by differentiation from the onboard compass. Note, however, that the contribution of the term b/R_t is typically very small and practically β can be confused with α_r, when also δ_r is null.

2) Trace tracking: The FTrace module performs three main tasks:

- Extraction of trace candidates from the scene.
- Estimation of their pose with respect to the camera, i.e. the vehicle, reference frame.
- Selection of the candidate that best fits to the trace model.

In the reminder of this section each phase is described in detail.

***Trace extraction* —** Each image is processed following two steps. First, an optimized Canny's edge detection [17] is performed. Then, Hough transform [18], is applied to extract lines from the scene. Edges in images are areas with strong intensity contrasts. Edge detection significantly reduces the

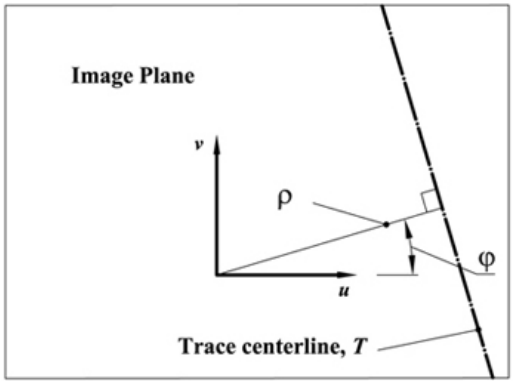

Fig. 3. Model of the trace of the wheel in the image plane. Note that the parameter ρ is expressed in pixels

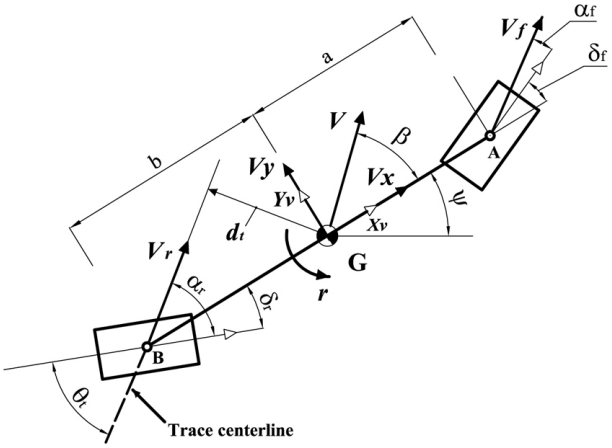

Fig. 4. Model of the trace in the real world with reference to a bicycle schematization of the robot

amount of data and filters out useless information, while preserving the important structural properties of the objects in the scene. The Canny's operator is based on a 3×3 Sobel kernel and the Low Threshold (LT) and High Threshold (HT) hysteresis were well experimentally determined as

$$LT = \frac{I_{max} - I_{min}}{3} \tag{3}$$

$$HT = 2.5 \cdot LT \tag{4}$$

where I_{max} and I_{min} are the maximum and minimum intensity value, respectively, detected in the current frame. Ideally, edge detection is able to identify object boundaries. However, because of noise, non-uniform illumination, and other spurious effects, this technique usually fails to characterize edges completely. Hence, edge linking methods must be used to assemble pixels into meaningful edges. One of the most known edge linking methods is the Hough transform, which allows one to fit lines to the edges, detected by Canny's operator. At the end of the Hough transform application, a set of trace candidates will be available.

***Pose Estimation* —** Once the perspective projection of the candidate trace has been determined in the image plane, its pose can be estimated in the vehicle frame. The following assumptions hold

- The candidate trace has been detected and the coordinates of its points are known in the image plane.
- The intrinsic and extrinsic camera parameters have been previously determined through the application of a calibration method.

With reference to Fig. 5, three reference frames can be considered: a 3D World Reference Frame (WRF) $\{w, X_w Y_w Z_w\}$, a 3D Camera Reference Frame (CRF) $\{c, X_c Y_c Z_c\}$, and a 2D Image Reference Frame (IRF) $\{o, uv\}$. The CRF is characterized by the axis Z_c coincident with the optical axis and the other two axes parallel to the image plane. The IRF is centered in the principal point o, which is defined as the intersection between the optical axis and the image plane. A given point P of the scene is projected onto the image plane in the point P', according to the classical camera pinhole model [19]. If we denote with $P^c = (P_x^c, P_y^c, P_z^c)$ the coordinates of P in the CRF, we can estimate its projection on the image plane as

$$u = -f_u \cdot \frac{P_x^c}{P_z^c} \tag{5}$$

$$v = -f_v \cdot \frac{P_y^c}{P_z^c} \tag{6}$$

where u and v are the coordinates of P' in pixel units, and f_u and f_v are the focal length in pixel units evaluated along the horizontal and vertical direction of the image plane, respectively. The position of P with respect to the WRF $P^w = (P_x^w, P_y^w, P_z^w)$, can be determined as

$$P^w = R_c^w P^c + t_c^w \tag{7}$$

where R_c^w is the rotation matrix of the CRF with respect to the WRF, and t_c^w represents the coordinates of the origin c of the CRF in the WRF. The rotation matrix R_c^w can be expressed in terms of a set of three independent angles known as Euler angles. In our implementation, we adopted the so-called ZYX Euler angles ϕ, θ and ψ, which are usually referred to as roll, pitch and yaw angle, respectively

$$R_c^w = \begin{pmatrix} c_\psi c_\theta & c_\psi s_\theta s_\phi - s_\psi c_\phi & c_\psi s_\theta c_\phi + s_\psi s_\phi \\ s_\psi c_\theta & s_\psi s_\theta s_\phi + c_\psi c_\phi & s_\psi s_\theta c_\phi - c_\psi s_\phi \\ -s_\theta & c_\theta s_\phi & c_\theta c_\phi \end{pmatrix} \tag{8}$$

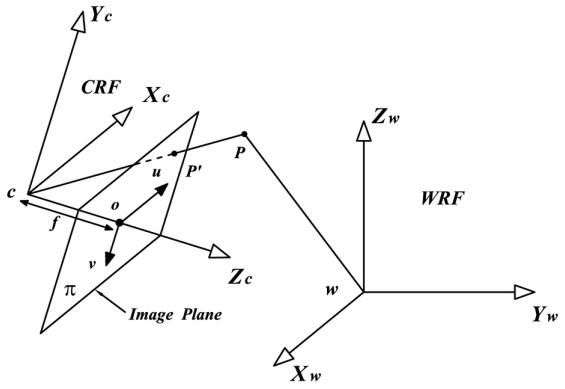

Fig. 5. Nomenclature for the reference frames

where the notations c_ϕ and s_ϕ are the abbreviations for $cos\phi$ and $sin\phi$, respectively. We can now write explicitly (7) as

$$P_x^w = r_{11} \cdot P_x^c + r_{12} \cdot P_y^c + r_{13} \cdot P_z^c + t_x \quad (9)$$

$$P_y^w = r_{21} \cdot P_x^c + r_{22} \cdot P_y^c + r_{23} \cdot P_z^c + t_y \quad (10)$$

$$P_z^w = r_{31} \cdot P_x^c + r_{32} \cdot P_y^c + r_{33} \cdot P_z^c + t_z \quad (11)$$

where r_{ij} are the components of the rotation matrix R_c^w. Without loss of generality, we can assume the x-axis of the WRF, i.e. X_w, to be coincident with the trace of the wheel. Under this assumption, a given point $\bar{P}$ belonging to the trace will have coordinates in the WRF $\bar{P}^w = (\bar{P}_x^w, 0, 0)$. The transformation between the WRF and the CRF can be obtained using (5), (6), and (11); they form a set of three equations in three unknowns, i.e. the coordinates of $\bar{P}$ in the CRF $\bar{P}^c = (\bar{P}_x^c, \bar{P}_y^c, \bar{P}_z^c)$, being the coordinates u and v given from the previous step of the algorithm, and the extrinsic parameters t_z, i.e. the vertical component of vector t_c^w, ϕ, and θ known from the camera calibration. Note that the extrinsic parameters are assumed to undergo small changes in their value during operation and thus considered constants in our algorithm. This is a reasonable hypothesis for navigation on loose surfaces and for line-like landmarks located on the ground [20], as also demonstrated by the sensitivity analysis of the system discussed later in Section III-C. By repeating this procedure for at least two points belonging to the trace, it is possible to obtain its equation in the CRF. Finally, the pose of the trace can be referenced to the VRF through a simple geometrical transformation to obtain the parameters of interest θ_t and d_t, as previously defined in Section II-A.1.

Trace selection — In order to determine which line best fits to the trace model we use fuzzy reasoning [21]. The general approach is based on comparing the geometrical properties of each candidate with those of the trace model, (as defined in Section II-A.1), in both the image plane and the real world, and defining deterministic conditions for model matching. The output of the FTrace is a fuzzy quantity that expresses the certainty that the line agrees exactly with the trace model. Given n lines (e.g., n=10) extracted from the image i and generally denoted as T_j^i (e.g., j = 1, 2,.., n), one can compute their pose in the image plane $P_j^i = (\rho_j^i, \varphi_j^i)$, and compare it with that of the trace marker obtained in the previous frame, namely $P^{i-1} = (\rho^{i-1}, \varphi^{i-1})$. Under the assumption of relatively small displacement of the trace with respect to the robot between two consecutive images frames, P^{i-1} can be regarded as a good reference value. If the trace pose P_j^i agrees with P^{i-1}, then one can expect good correspondence between that line and the trace model. Poor correspondence suggests low likelihood of matching. Similarly, the pose of the trace candidate T_j^i in the real world $R_j^i = (d_j^i, \theta_j^i)$ can be compared with that estimated in the previous frame $R^{i-1} = (d^{i-1}, \theta^{i-1})$. Small change in the distance and orientation value suggests high likelihood of matching of the candidate with the model. Note that it is important to perform this comparison in both spaces to check the physical consistency of the candidates obtained from the previous image segmentation. Finally, in the real world, the candidate T_j^i must also fulfill the geometrical constraint of passing through the center of the wheel, namely point B in Fig. 4. With reference to the same figure, one can compute the intersection Y_j^i of the candidate T_j^i with the parallel to the axis Y_v through point B, and the distance of Y_j^i from the center of the wheel as $\Delta Y_j^i = |Y_j^i - Y_B|$, where Y_B is the coordinate of B along Y_v. If the discrepancy is small, then one can expect good agreement with the model. Conversely, large values of ΔY_j^i suggest poor confidence of matching.

We express these hypotheses with fuzzy logic that uses rules to map from inputs to outputs. The membership functions of the inference system are shown in Fig. 6. They were chosen triangular based on the authors' experience, and their thresholds were determined experimentally. The fuzzy data fusion uses five inputs and one output. The inputs are the geometrical data, i.e., the absolute difference in distance and orientation estimated in the image plane, denoted with $\Delta\rho_j$ and $\Delta\varphi_j$ respectively, and in the real world, denoted with Δd_j and $\Delta\theta_j$ respectively, between the candidate pose and the model pose in the previous frame, and the distance ΔY_j^i of the candidate from the wheel center B. The output is a dimensionless factor, ranging from zero to one, which expresses the degree of confidence we have that the candidate matches the trace model. The fuzzy inference system fuses the geometrical information based on the *if-then* rule set shown in Table I. Those rules express our physical understanding of the phenomenon and they were chosen to give the best performance over other alternatives using a trial and error process. The rule set is not unique; new rules may be thought of and implemented adopting more sophisticated optimization methods to improve the performance of fuzzy inference systems [22], [23]. However, the accuracy of the FTrace system is already adequate for the application, as shown by the experimental results presented later in Section III, and further refinement of the fuzzy reasoning would lead to a small or negligible improvement at the price of greater computational complexity.

B. Experimental Analysis

Representative experimental results of the FTrace module are shown in Fig. 7 for a sample image grabbed during a field trial of El Dorado on sandy surface. After the trace extraction stage of the algorithm, ten candidates were extracted by the system, as shown in Fig. 7(b) and Fig. 7(c). The successive trace selection stage provided the confidence

TABLE I
FUZZY LOGIC RULES USED BY THE FTRACE MODULE

Rule	Input:					Output:
#	$\Delta\rho_j$	$\Delta\varphi_j$	Δd_j	$\Delta\theta_j$	ΔY_j^i	Confidence Match
1	Small	Small	Small	Small	Small	High
2	Small	Large	Small	Large	Small	Med.
3	Large	Small	Large	Small	Large	Low
4	Large	Large	Large	Large	Large	Low
5	Large	Large	Small	Small	Large	Low
6	Small	Small	Large	Large	Small	Med.

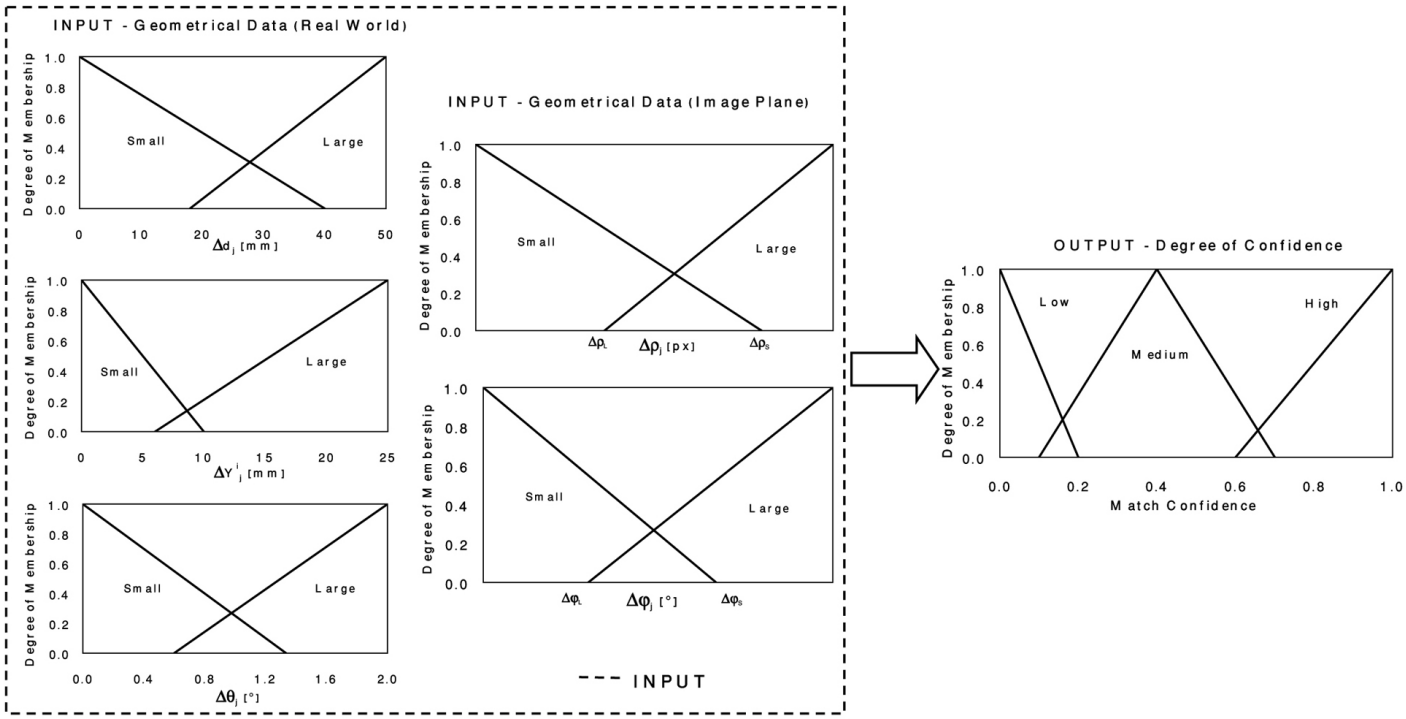

Fig. 6. Membership functions of the FTrace system

TABLE II
DEGREE OF CONFIDENCE IN MODEL MATCHING FOR THE TRACE CANDIDATES OF FIG. 7 AS DERIVED FROM THE FTRACE SYSTEM

Candidate Line #	L_1	L_2	L_3	L_4	L_5	L_6	L_7	L_8	L_9	L_{10}
Confidence Match %	4.1	1.1	1.3	1.4	89.0	9.1	20.0	20.3	18.7	20.2

matches collected in Table II. The lane marker, denoted with L_5 in Fig. 7(b) and shown by a dotted blue line in Fig. 7(c), yielded the greatest confidence level (89%), and was therefore selected as the best match. In Fig. 7(d), the output of the FTrace system is overlaid over the original scene along with the estimated values of d_t and θ_t.

III. EXPERIMENTAL RESULTS

In this section experimental results are presented, aiming at assessing the overall effectiveness of the FTrace method in the field. The system was integrated with the rover El Dorado using a cost-effective rear webcam and a sampling rate of 5 Hz. The webcam was calibrated using the Matlab camera calibration toolbox [24]. The test field was located on the shoreline of a sandy beach, comprising large flat areas and sparse mounds of different extensions and heights. In all experiments, the rover was remotely controlled, using a wireless joypad to follow a straight-line path with a travel speed of about 8 cm/s. Two types of environment were considered:

- Set A: sandy relatively flat terrain. These experiments were aimed at evaluating undue errors of the FTrace system incurred by low-slippage terrain.
- Set B: sandy non-flat terrain, including driving uphill or sideways on sandy slopes with substantial lateral slip.

The entire experimental area was within the range of a laser-based absolute positioning system that provided the ground-truth translational position (x, y, z) with respect to a global coordinate frame. The ground-truth sideslip angle of the robot β_g was estimated as the difference between the absolute vehicle heading direction ψ_l, derived by the laser position-measurement system, and the vehicle heading ψ, measured by the onboard compass

$$\psi_l = \arctan(\frac{\dot{y}}{\dot{x}}) \tag{12}$$

$$\beta_g = \psi_l - \psi \tag{13}$$

A. Robustness Analysis

The FTrace system was tested over a total of 15016 images showing the results collected in Table III obtained from both sets of experiment. Figure 8 also shows some typical results obtained from sample images of different tests. The percentage of false positives, i.e. a trace marker detected when actually there is no trace marker, was less than 0.3% and limited to the initial moments of the robot's motion. Conversely, false negatives arise when the trace marker is

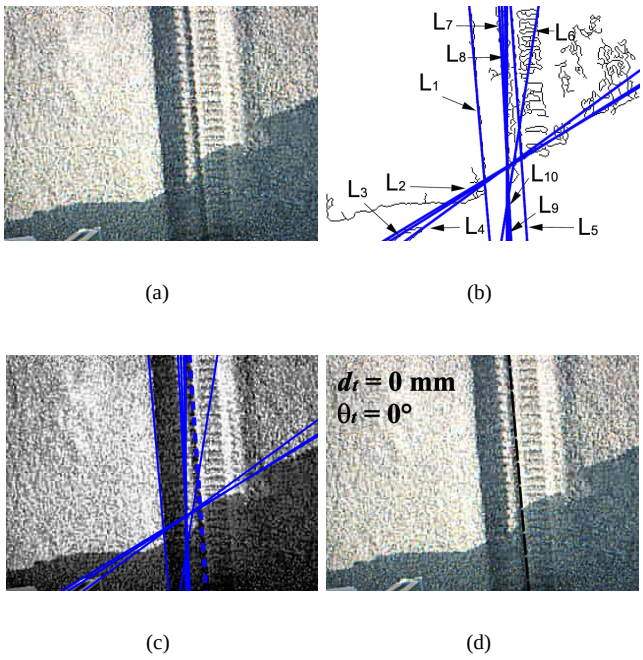

Fig. 7. Application of the FTrace system to a sample image: (a) original scene, (b) and (c) application of edge detection and Hough transform, (d) output of the FTrace system. Note that for this image no sideslip was detected

present in the image but the system is not able to detect it at all and does not return any information. The percentage of false negatives was less than 3%, and due largely to poor image segmentation and camera calibration errors (80%), and model approximation (20%). As an example, Fig. 9 and Fig. 10 show two scenes where the FTrace system failed. Finally, misidentifications refer to cases in which a trace marker is present in the image but the system fails in recognizing it properly and returns wrong information. In all tests, misidentifications were less than 1%. Overall, the system proved to be robust to disturbances due to heavy shadowing, non-uniform terrain texture, and the presence of overlapping imprints. Note that, the knowledge of the pose of the trace in one image is used to determine the region of interest (ROI) to be searched for model detection in the next frame. This makes the trace search more accurate and reduces computational requirement by eliminating much of the scene, as shown by the second and third column of Fig. 8, and the second column of Fig. 9 and Fig. 10. In the first column of the same figures, the detected trace and the output of the FTrace system is overlaid over the original image.

B. Accuracy Analysis

In order to assess the effectiveness of the FTrace system in estimating lateral drift, the results obtained in a typical test on non-flat terrain are presented. In this experiment, El Dorado was commanded to move straight forward up a 5-degree sandy slope including various sparse mounds, resulting in a total travel distance of about D=13 m. Figure 11 shows the position of El Dorado and the imprints produced by its wheels at the end of the run, from a front and rear view, respectively. The slip angle, derived from the FTrace system using (2), is compared with the ground-truth data in Fig. 12. The two curves show good agreement with a root mean square (RMS) error less than 2 deg. The FTrace system detected effectively the onset of sideslip and its trend throughout the experiment. In the initial stage of its traverse, about first 60 seconds, the rover followed the planned path as demonstrated by the two wheel traces parallel to the direction of motion. Afterward, El Dorado experienced two large drifts incurred by changes in the transverse inclination of the terrain producing lateral force disturbances. As a direct consequence, a change in the pose of the wheel traces can be observed (see Fig. 11), attesting to the feasibility of the proposed approach. Since the accuracy of the FTrace method was consistent in all the experiments of both set A and B, this result can be regarded as of general significance.

C. Sensitivity Analysis

The extrinsic parameters of the camera, estimated through an initial calibration, can change during operation due to the deformability and unevenness of the terrain. In order to study the system's sensitivity to these parameters, all experimental data sets were reprocessed varying the value of the constants both individually and combined. Specifically, a change of 5% in the value of t_z, namely the height of the camera from the ground, was considered on an individual basis. This corresponds to an expected maximum sinkage of the wheel into the soil of about half of its radius (R=50 mm). Variations in the value of the pitch and roll angle of the rover were also assumed individually in the order of $\pm 10\,\mathrm{deg}$ from the nominal value. A combined variation of roll and pitch was also studied with a change of 5 deg and 10 deg, respectively. The results are summarized in Table IV expressed in terms of percentage of false negatives and error N_{RMS} in the estimation of slip angle relative to the nominal performance of the FTrace system. The variations in the percentage of false positives and misidentifications is of lesser significance and omitted. The effect of height change of the camera was negligible on the accuracy of the system with a slight increase in the total number of false positives from 336 (2.7%) to 361 (2.9%). Also negligible was the influence of individual change in the roll angle since the output of the FTrace system is invariant for rotation about the longitudinal axis of the rover (see Section II-A.2). Conversely, single variations of pitch and combined variations of pitch and roll affect the performance of the system in terms of both accuracy and number of false positives with a worst-case

TABLE III

RESULTS OBTAINED FROM THE FTRACE SYSTEM FOR DIFFERENT TERRAINS. SET A: FLAT SANDY TERRAIN, SET B: NON-FLAT TERRAIN

Set #	Frames	False Positives (%)	False Negatives (%)	Misid.(%)
A	2560	0.1	1.5	0.0
B	12456	0.2	2.7	0.8

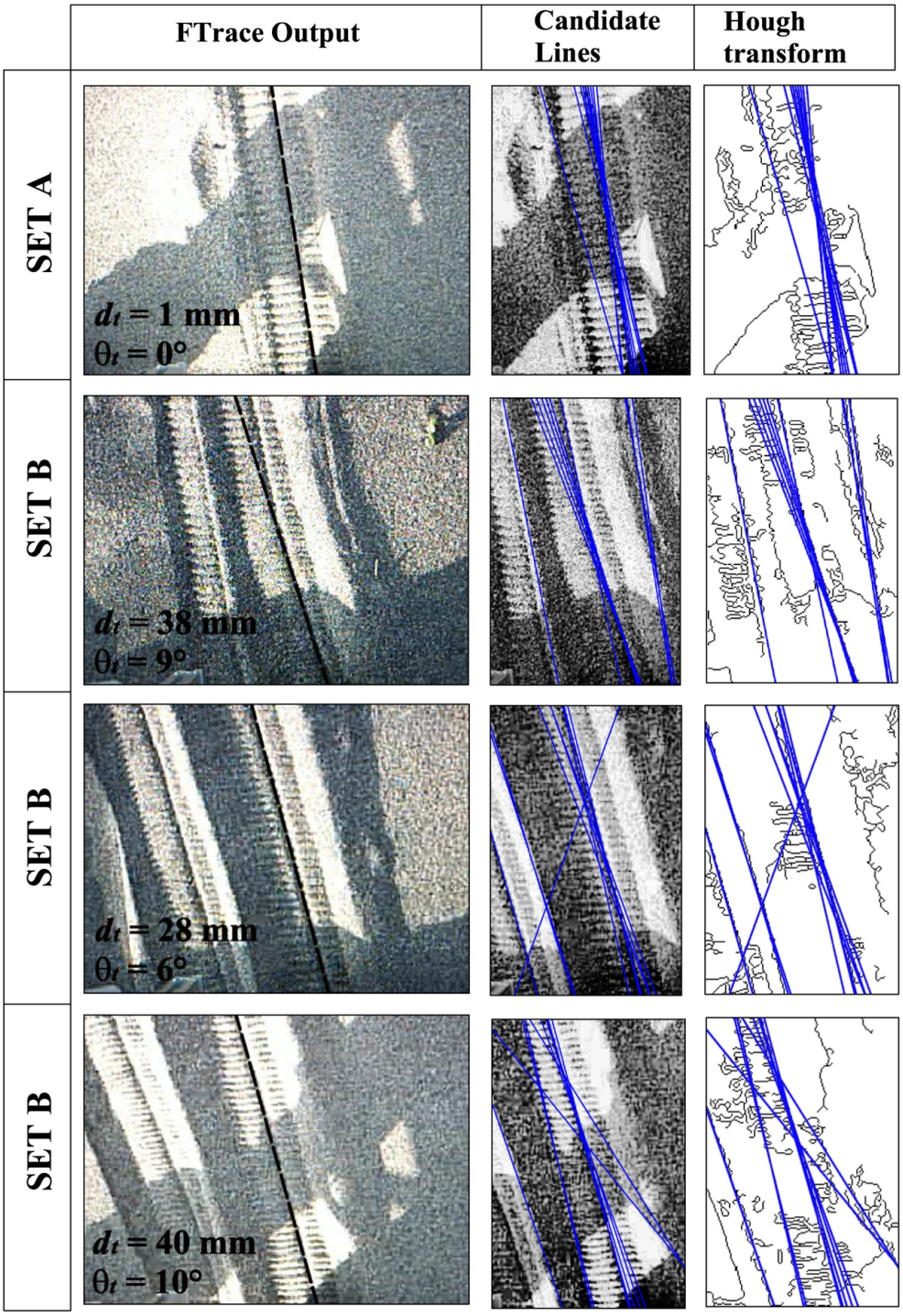

Fig. 8. Results obtained from the FTrace system under various terrain and environmental conditions. See Table III for more details

error in the estimation of slip angle of 2.8 deg and a number of false positives of 897 (7.2%). Note however that these errors could be corrected on-line by measuring the tilt of the rover during operation, using for instance an onboard IMU. In summary, the algorithm appears quite robust to errors in the extrinsic parameters.

IV. Conclusions

In this paper, a novel method for sideslip estimation was presented based on observing the wheel traces left by a robot during its traverse of loose terrains. A visual algorithm was proposed to estimate the pose of the traces using a Hough transform enhanced by fuzzy reasoning. The important geometrical data of the scene are combined based on the physical understanding of the problem providing accuracy and robustness. Comprehensive experiments in the field demonstrated the overall effectiveness of the proposed FTrace method for slip angle estimation on sandy terrain with a percentage of failed observations less than 3% and

TABLE IV

SENSITIVITY OF THE PERFORMANCE OF THE FTRACE SYSTEM TO CHANGES IN THE EXTRINSIC PARAMETERS. THE NOMINAL PERCENTAGE OF FALSE NEGATIVES IS 2.7%. N_{RMS} IS THE ERROR RELATIVE TO THE NOMINAL ACCURACY, I.E. E_{RMS} = 1.6°, SEE SECTION III-B FOR MORE DETAILS

Parameter	Nominal	Change	False Negative (%)	N_{RMS} (°)
t_z (mm)	488	+25	2.9	0.3
		-25	2.9	0.2
Roll ϕ (°)	0	+10	2.7	0.0
		-10	2.7	0.0
Pitch θ (°)	0	+10	6.5	2.6
		-10	6.0	1.7
ϕ (°)	0	+5	7.2	2.8
θ (°)	0	+10		

an accuracy of 1.6 deg. A sensitivity analysis was also discussed proving the robustness to uncertainties of the model. The FTrace module could be effectively employed to enhance the mobility of robots on highly challenging terrains by integration with conventional control and localization algorithm.

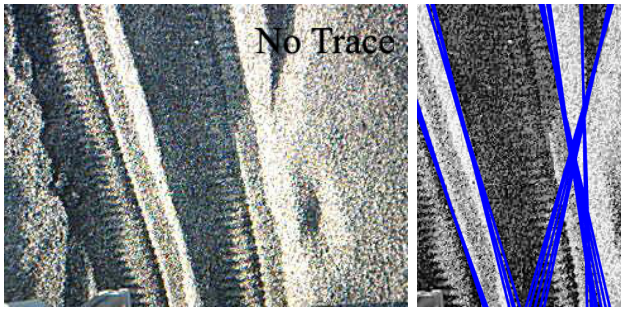

(a) (b)

Fig. 9. Example of false negative due to poor image segmentation (a) FTrace output, (b) trace extraction stage

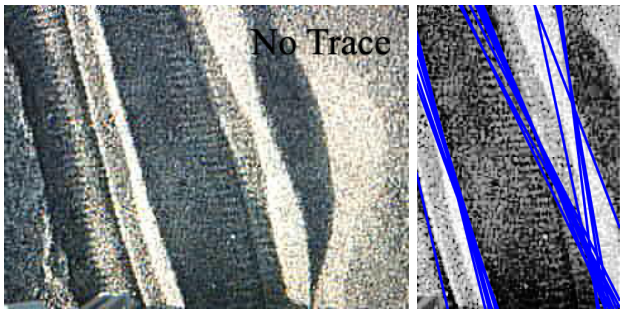

(a) (b)

Fig. 10. Example of false negative due to model approximation (a) FTrace output, (b) trace extraction stage

(a) (b)

Fig. 11. Traces produced by the wheels of the rover at the end of the traverse of a sandy slope: (a) front view, (b) rear view

V. ACKNOWLEDGMENTS

The authors would like to thank Dr. Keiji Nagatani and Genya Ishigami for their help performing experiments, and Dr. Annalisa Milella for the precious discussions on the visual algorithms. The authors are also thankful to the Japanese Society for the Promotion of Science for supporting the project through Fellowship P06061.

REFERENCES

[1] M. Maimone, Y. Cheng, and L. Matthies, "Two Years of Visual Odometry on the Mars Exploration rovers," Journal of Field Robotics, vol. 24, no. 3, pp.169-186, 2007.

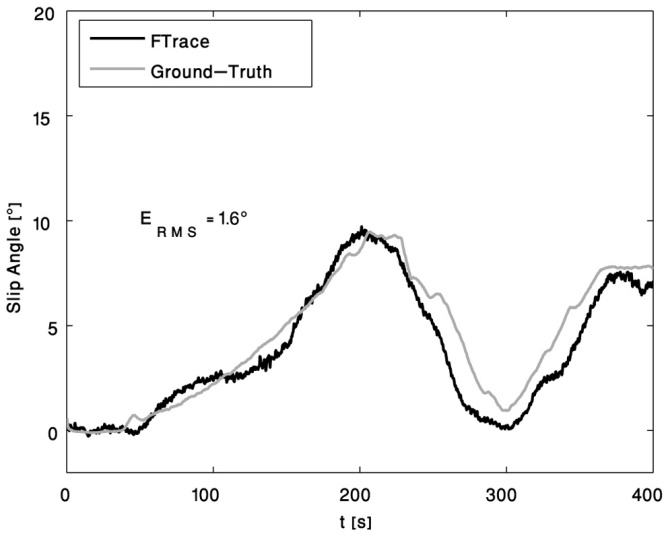

Fig. 12. Accuracy of the FTrace system in estimating slip angle for a traverse of a sandy slope including sparse mounds

[2] T. Huntsberger et al., ”Rover Autonomy for long Range Navigation and Science Data Acquisition on Planetary Surfaces,” in Proc. IEEE Int. Conf. on Robotics and Automation, Washington, DC, 2002.
[3] F. Gustafsson, ”Slip-based tire-road friction estimation,” Automatica, vol. 33, no. 6, pp. 1087-1099, 1997.
[4] G. Reina, L. Ojeda, A. Milella, and J. Borenstein, ”Wheel Slippage and Sinkage Detection for Planetary Rovers,” IEEE/ASME Transactions on Mechatronics, vol. 11, no. 2, April, 2006.
[5] L. Ojeda, D. Cruz, G. Reina, J. Borenstein, ”Current-based slippage detection and odometry correction for mobile robots and planetary rovers,” IEEE Transactions on Robotics, vol. 22, no. 2, April 2006.
[6] C. Ward, and K. Iagnemma, ”Model-based Wheel Slip Detection for Outdoor Mobile Robots,” In Proc. IEEE Int. Conf. on Robotics and Automation, Rome, Italy, April 2007.
[7] G. Ishigami, A. Miwa, K. Nagatani, and K. Yoshida, ”Terramechanics-based Model for Steering Maneuver of Planetary Exploration Rovers on Loose Soil,” Journal of Field Robotics, vol. 24, no.3, pp.233-250, 2007.
[8] H. Tan, Y. Chin, ”Vehicle antilock braking and traction control: a theoretical study,” Int. J. of Systems Science, vol. 23, no. 3, 1992.
[9] Automotive Handbook, 5th ed., Robert Bosch GmbH, Germany, 2000.
[10] R. Anderson, D Bevly, ”Estimation of slip angles using a model based estimator and GPS,” In Proc. of American Control Conf., vol. 3, 2004.
[11] J. Hahn, R. Rajamani, L. Alexander,”GPS-based Real-Time Identification of Tire-Road Friction Coefficient,” IEEE Transactions on Control Systems Technology, vol. 10, No. 3, May 2002.
[12] S. Sukkarieh, E. Nebot, H. Durrant-Whyte, ”A high integrity IMU/GPS navigation loop for autonomous land vehicle applications,” IEEE Trans. on Robotics and Automation, vol. 15, no. 3, June 1999.
[13] J.C. McCall and M.M. Trivedi, ”Video-based Lane Estimation and Tracking for Driver Assistance: Survey, System, and Evaluation.” IEEE Transactions on Intelligent Transportations Systems, Vol. 7, No.1, 2006.
[14] C. Taylor, J. Koeck, R. Blasi, and J. Malik, ”A comparative study of vision-based lateral control strategies for autonomous highway driving,” Int. J. Robot. Res., vol. 18, no. 5, pp. 442-453, May 1999.
[15] A. Milella, G. Reina, ”A Fuzzy Lane Tracking System for Driver Assistance,” Proc. ASME Int. Mechanical Engineering Congress and Exposition, Chicago, Usa, November 2006.
[16] G. Genta, Motor Vehicle Dynamics. World Scientific Publishing, Singapore, 2003.
[17] J. Canny, ”A Computational Approach to Edge Detection,” IEEE Transactions on Pattern Analysis and Machine Intelligence, Vol. 8, No. 6, 1986.
[18] P. Hough, ”Methods and Means for Recognizing Complex Patterns”, U.S. Patent, n. 3069654, 1962.
[19] R. Gonzales, and R. Woods, ”Digital Image Processing”, Prentice Hall, 2007.
[20] A. Milella, ”Vision-Based Methods for Autonomous Mobile Robots”, PhD Thesis, Politecnico of Bari, Italy, 2006.
[21] J. M. Mendel, ”Fuzzy Logic Systems for Engineering: A Tutorial,” IEEE Proceedings, vol. 83, no. 3, 1995.
[22] S. E. Woodard, and D. P. Garg, ”A numerical optimization approach for tuning fuzzy logic controllers,” IEEE Transactions on Systems, Man, and Cybernetics: Part B, Vol. 29, No. 4, 1999, pp. 565-569.
[23] W. Pedrycz, and J. V. Oliveira, ”An Algorithm Framework for Development and Optimization of Fuzzy Models,” Fuzzy Sets and Systems, Vol. 80, 1996, pp. 37-55.
[24] J. Bouguet, ”Camera Calibration Toolbox for Matlab,” available on line at: http://www.vision.caltech.edu/bouguetj/calib_doc/

Giulio Reina received the *Laurea* degree and the *Research of Doctorate* degree from the Politecnico of Bari, Italy in 2000 and 2004 respectively, both in Mechanical Engineering. From 2002 to 2003, he worked at the University of Michigan Mobile Robotics Laboratory as a Visiting Scholar. In 2007, he was awarded a Japanese Society for Promotion of Science (JSPS) fellowship for a one-year research stay at the Space Robotics Laboratory of the Tohoku University, Sendai, Japan. Currently, Dr. Reina is an Assistant Professor in Applied Mechanics with the Department of Innovation Engineering of the University of Salento, Lecce, Italy. His research interests include planetary rovers, mobility and localization on rough-terrain, computer vision applied to robotics, and agricultural robotics.

Kazuya Yoshida received B. E. and M. S. degrees in mechanical engineering science from Tokyo Institute of Technology, Japan, in 1984 and 1986, respectively. He received Dr. Eng. from Tokyo Institute of Technology in 1990. He served as a research associate of Tokyo Institute of Technology from 1986 to 1994, and a visiting scientist of Massachusetts Institute of Technology, U.S.A. in 1994. From 1985 to 2003, he was appointed as an associate professor of Tohoku University, Japan and since 2003 a professor in Department of Aerospace Engineering, Tohoku University. He is also serving as a visiting lecturer of International Space University since 1998. His research activities include dynamics and control issues of various types of space robots covering from free-flying robots to planetary exploration rovers. Recently his activities have been extended to terrestrial applications of space technology, such as telerobotics for disaster mitigation missions.